Journal of The Electrochemical Society, 2020 **167** 120544
1945-7111/2020/167(12)/120544/10/$40.00 © 2020 The Electrochemical Society ("ECS"). Published on behalf of ECS by IOP Publishing Limited

Analytical Model Based Prediction of State-of-Charge (SoC) of a Lithium-Ion Cell under Time-Varying Charge/Discharge Currents

Mohammad Parhizi,[1] Manan Pathak,[2] and Ankur Jain[1,z]

[1]*Mechanical and Aerospace Engineering Department, University of Texas at Arlington, Arlington, Texas, United States of America*
[2]*BattGenie, Inc., Seattle, Washington, United States of America*

Real-time State of Charge (SoC) estimation of a Li-ion cell is necessary for an accurate estimation of the state of the cell, and to ensure safety and efficient performance by avoiding overcharge or overdischarge. While past papers have presented analytical models for predicting voltage and SoC for constant-current conditions, there is a need for analytical models that account for time-varying charge/discharge currents representative of realistic conditions. This paper presents an analytical SPM-based model to predict the terminal voltage and SoC of a Li-ion cell operating under a general time-dependent current profile. Concentration distributions in the positive and negative electrodes are determined analytically using Green's function approach, followed by determination of the electrode voltages as functions of time using the Butler–Volmer kinetic equation. The analytical model is validated through good agreement with numerical simulations and past experimental data for a number of different operating conditions. Cell voltage and SoC are predicted for a variety of time-varying currents, including drive cycles representative of realistic driving conditions. It is expected that the analytical model developed here will help improve the performance of battery management systems by obtaining more accurate information about the internal state of the cell in realistic charge/discharge conditions.
 [DOI: 10.1149/1945-7111/abb34d]

Manuscript submitted July 9, 2020; revised manuscript received August 10, 2020. Published September 7, 2020.

List of symbols

c	concentration (mol m^{-3})
$c_{initial}$	initial concentration (mol m^{-3})
c_{max}	maximum concentration (mol m^{-3})
c_e	electrolyte concentration (mol m^{-3})
D	diffusion coefficient ($m^2 s^{-1}$)
F	Faraday constant (96485 C mol^{-1})
I	current (A)
J	molar flux (mol m^{-2} s^{-1})
k	reaction rate constant ($m^{2.5}$ $mol^{-0.5}$ s^{-1})
r	radial spatial coordinate (m)
R	particle radius (m)
R_u	universal gas constant (8.314 J mol^{-1} K^{-1})
R_{cell}	cell resistance (Ω)
S	total electroactive area (m^2)
t	time (s)
U	open circuit potential (V)
V	total volume of the electrodes (m^3)
V_{cell}	Cell Voltage (V)
x	stoichiometric or scaled concentration
ε	volume fraction of the active material in electrode
η	overpotential (V)
λ	eigenvalue (m^{-1})
ω	frequency (hr^{-1})
ϕ	potential (V)

Li-ion cells are an attractive candidate for electrochemical energy storage and conversion in electric vehicles (EVs) and power grids.[1] In such applications, managing the health and safety of Li-ion cells is very important, particularly for high power applications with significant demand variability. Battery Management Systems (BMS) using battery models of varying levels of complexity are commonly used to monitor and control the state of the cells, and to fulfill system design requirements.[2–4]

The State of Charge (SoC) of a cell is one of the most important variables that needs to be estimated frequently by the BMS. SoC has been defined in several different ways, such as an indication of the fraction of energy left in the battery at a given time, or the ratio of the available capacity to the maximum capacity of the cell at a given time.[2,5] An accurate estimate of the SoC helps infer useful information about the vehicle range, remaining energy and health of the battery pack.[5,6] Unlike electric parameters such as voltage and current, SoC cannot be measured directly and other methods must be implemented to obtain an accurate estimate of SoC.[7] Due to the coupled and non-linear nature of the electrochemical phenomena that occurs in Li-ion cells, SoC estimation is always a challenging task.[5] While SoC estimation for constant current processes may be relatively easier, it is a much more complicated task under dynamic load conditions, as one would expect, for example, in an electric vehicle.

A variety of techniques have been proposed in the literature to evaluate SoC of Li-ion cells. State of charge estimation techniques can be broadly divided into the categories of non-model based techniques, data-driven (machine learning) approaches and model-based techniques.[5,8,9]

One example of non-model based techniques is the open-circuit voltage (OCV) method that uses a look-up table based on a monotonic relationship between SoC and open-circuit voltage.[10] This method is not suitable for SoC estimation in electric vehicles since an accurate real-time measurement of OCV is not straightforward.[5,11] Also, the flat nature of OCV behavior of certain cathode chemistries used in Li-ion batteries, such as Lithium Iron Phosphate makes it unsuitable to accurately estimate the SoC at all times. In the Ampere-hour integral method, also known as the Coulomb counting method, SoC is estimated by integrating the current over time.[8,12] This method can be fairly accurate as long as the initial SoC, cell maximum capacity and electric current are precisely known.[5,13] However, any inaccuracy in the initial SoC along with noise in the current measurements can significantly affect the accuracy of SoC prediction.

Data-driven methods use large sets of experimental data obtained under different operating conditions to build a pattern and demonstrate a relationship—often non-linear—between different input and output variables.[5,14] Fuzzy logic,[15] autoregressive moving average (ARMA),[16] artificial neural network (ANN)[17] and support vector machine (SVM)[18] are key data-driven methods.[14] Data-driven methods are often computationally expensive, and the accuracy depends strongly on the size and quality of the statistical population.

Model-based methods can be broadly divided into equivalent circuit models (ECMs) and electrochemical models. ECM uses a

[z]E-mail: jaina@uta.edu

circuit network comprising of capacitors, resistors and other electrical circuit components to simulate battery behavior.[5,19] Compared to electrochemical models, ECMs are simpler and faster, but do not provide insights on electrochemical processes occurring inside the cell.[2] Estimation algorithms such as Kalman filter,[20–23] extended Kalman filter,[24] voltage inversion technique,[25] sliding mode observer,[26] and Luenberger observer[27] have been used with ECM techniques.

Electrochemical models, on the other hand, provide a robust and detailed solution by solving reaction kinetics, mass and charge transport equations under appropriate assumptions. Pseudo-two dimensional model (P2D) proposed by Doyle et al.[28] has been used widely in modeling of Li-ion batteries,[29,30] particularly for understanding the effect of design parameters on cell energy and power.[31] 1-D electrochemical model has been also used to predict the SoC of Li-ion cells.[32–34] Due to the coupled and non-linear nature of the partial differential equations (PDEs) that the P2D models solve, the equations usually need to be solved numerically, which is computationally expensive. Several researchers have proposed reduced-order models to simplify the computational complexity. Recently, a lumped electrochemical model for lithium-ion batteries called Tank-in-Series approach has been introduced, in which the governing equations of the P2D model are volume-averaged over each region of the cell.[35] One of the most commonly used simplifications is the single particle model (SPM),[36] in which each electrode is replaced by a representative single, spherical particle, and the concentration distribution in the particle due to the imposed current is solved analytically or numerically. Compared to P2D, this results in only one PDE for each electrode. The current density is assumed to fully contribute towards the pore wall flux that is uniformly distributed throughout the surface of the electrode.[37,38] Moreover, concentration and potential gradients in the electrolyte is neglected. SPM is a valid approach only for low to moderate C-rate, where the concentration gradient in the electrolyte can be neglected.[37,38] At high current densities, the Li-ion concentration gradient and potential gradient in the electrolyte cannot be ignored and SPM results in inaccurate potential predictions.[39] A number of modifications of SPM have been proposed to overcome some of these limitations. For example, extended SPM model has been proposed to account for energy balance[37] and the effect of electrolyte concentration and potential.[8,40,41] Moreover, state estimation techniques such as an extended Kalman filter (EKF)[42] and Luenberger observer[34] has been applied to traditional and extended SPM to estimate the SoC of a Lithium ion cell.[42]

Regardless of the estimation technique, solving the concentration field in the spherical particle is a key step for SPM-based SoC estimation. Most analytical solutions for the diffusion equation governing the concentration field are applicable only for galvanostatic (constant current) operating conditions,[38] although a few papers have presented analytical solutions for time-dependent current density using Green's functions[43] and an approximate eigenfunction expansion with estimation of truncation error.[44] Even though step-wise changes in current can, in principle, be addressed by successively solving the concentration field in each galvanostatic time period, doing so is very difficult for rapidly changing current profiles encountered in vehicle drive cycles, or when the current changes smoothly over time, such as in alternating current (AC) systems. Previous studies have implemented a variety of numerical procedures and algorithms to predict the voltage and consequently SoC under dynamic discharge current conditions.[3,4] However, an analytical solution for determining the SoC during time-varying charge/discharge conditions is very desirable since it may offer the capability of rapid, in-line SoC estimation that integrates well with other BMS functions.

A Green's function based analytical solution for the concentration field in a single particle undergoing time-varying charge/discharge has recently been presented.[43] In the present paper, this analytical model is used to determine the voltage profile of the cell and the SoC as a function of time under a general, time-dependent current profile. The approach presented in this study results in an analytical expression for the voltage and SoC that can be used for any arbitrary time-dependent current profile. The analytical solution presented in this study is validated against past numerical simulations and experimental data under different operating conditions. The model is then used to predict the voltage and SoC of a Li-ion cell operating under realistic conditions such as drive cycles with rapidly changing charge/discharge current, as well as stepwise or periodically varying charge/discharge. While recognizing that the model presented here is valid only under the assumptions associated with the use of SPM, it is expected that the present study may contribute towards improved SoC estimation in a wide variety of applications containing extremely low-memory computational platforms where numerical solutions are impractical.

Mathematical Modeling

Solid phase diffusion.—Figure 1 shows a schematic of a unit Li-ion cell comprising of negative and positive electrodes, separator and current collectors. Also, a single spherical particle, representative of each electrode and the flow of ions during discharge process is shown. Single particle model (SPM) is used in the present study to predict the concentration profile in the electrodes. SPM neglects the concentration gradient in the solution phase and assumes the electrodes to comprise of spherical particles. Further, the assumption of a uniform current distribution results in identical conditions for each particle, so that a single spherical particle is representative of the entire electrode. It is important to note that these assumptions are valid for low current densities where the concentration gradient in the electrolyte can be neglected and the cell is dominated by solid phase diffusion. Under these assumptions, the governing equation for concentration diffusion for the positive and negative electrodes can be written as[38]:

$$\frac{D_j}{r^2}\frac{\partial}{\partial r}\left(r^2\frac{\partial c_j}{\partial r}\right) = \frac{\partial c_j}{\partial t} \quad [1]$$

where the initial and boundary conditions are

$$c_j = c_{initial,j} \quad \text{at } t = 0 \quad [2]$$

$$c_j \Rightarrow finite \quad \text{as } r \rightarrow 0 \quad [3]$$

$$D_j\left(\frac{\partial c_j}{\partial r}\right)_{r=R_j} = -J_j(t) \quad \text{at } r = R_j \quad [4]$$

where the subscript $j = p,n$ represents the positive and negative electrodes respectively. D is the solid phase diffusion coefficient and $J(t)$ is the time-dependent molar flux at the surface of the particle. The molar flux for the cathode and anode can be written as[38]:

$$J_p(t) = \frac{I(t)R_p}{3\varepsilon_p V_p F} \quad [5]$$

$$J_n(t) = -\frac{I(t)R_n}{3\varepsilon_n V_n F} \quad [6]$$

Where $I(t)$ is the current that is assumed to be time-dependent in this work, R_j is the radius of the particle electrode j. ε_j is the volume fraction of the active material in the electrode, V_j is the total volume, and F is the Faraday's constant. Note that the sign of the current, I, is negative for discharge and positive for charge.

Equations 1–6 have been recently solved analytically using Green's function approach for the case of time-dependent current. A detailed description of the solution procedure for solid phase diffusion under time-dependent boundary conditions can be found in a recent publication,[43] which results in the following equation for the

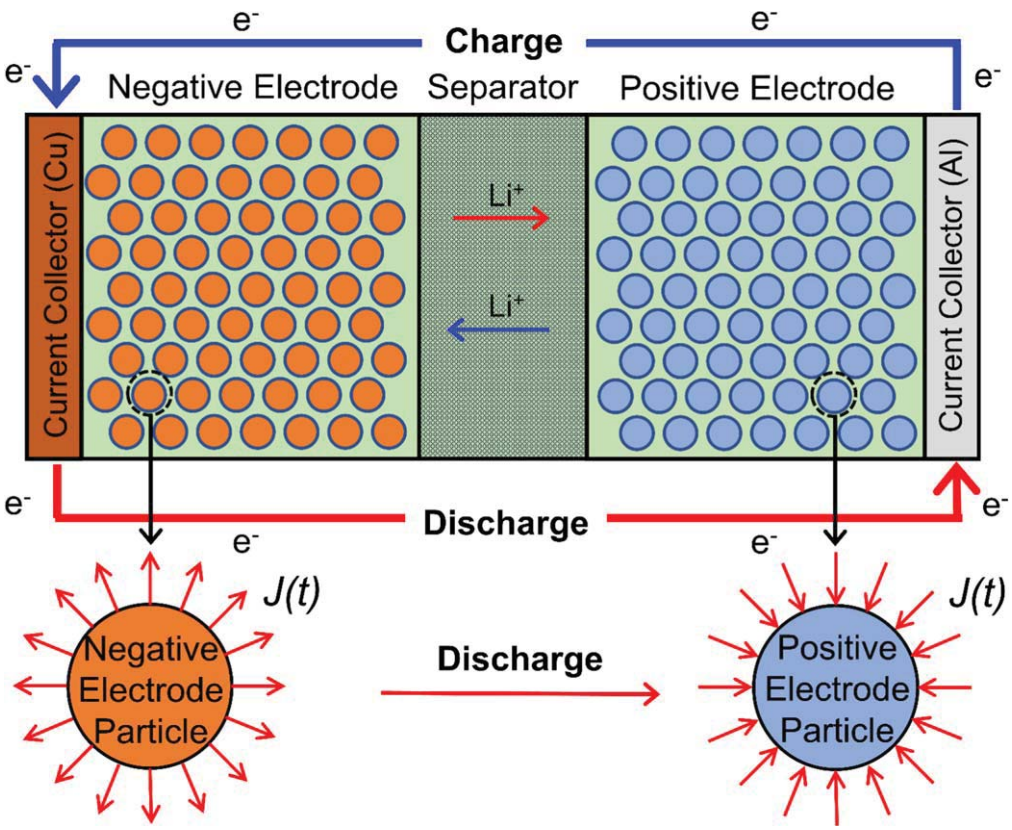

Figure 1. Schematic of a Li-ion cell comprising two electrodes, separator and current collectors. Two spherical particles representative of the two electrodes during discharge are also shown.

concentration distribution in the electrode particle[43]:

$$c_j(r,\,t) = c_{initial,j} - \frac{3}{R_j}\int_{\tau=0}^{t} J_j(\tau)d\tau - \sum_{n=1}^{\infty}\frac{R_j}{rN_{n,j}}\sin(\lambda_{n,j}r)\sin(\lambda_{n,j}R_j) \times \int_{\tau=0}^{t} J_j(\tau)\exp(-D_j\lambda_{n,j}^2(t-\tau))d\tau \quad [7]$$

where the eigenvalues, $\lambda_{n,j}$ are the positive roots of $R_j\lambda\cot R_j\lambda = 1$ and $N_{n,j}$ is the norm, defined as:

$$N_{n,j} = \frac{\lambda_{n,j}^2 R_j}{2\left(\lambda_{n,j}^2 + \frac{1}{R_j^2}\right)} \quad [8]$$

Specifically, concentration on the surface of the particle, which is important for calculating the potential can be determined by substituting $r = R_j$ in Eq. 7, resulting in:

$$c_{j,s}(t) = c_j(R_j,\,t) = c_{initial,j} - \frac{3}{R_j}\int_{\tau=0}^{t} J_j(\tau)d\tau - \sum_{n=1}^{\infty}\frac{1}{N_{n,j}}\sin^2(\lambda_{n,j}R_j) \times \int_{\tau=0}^{t} J_j(\tau)\exp(-D_j\lambda_{n,j}^2(t-\tau))d\tau \quad [9]$$

Potential and state of charge (SoC).—Once the concentration profile is determined for an arbitrarily varying charge/discharge current, the cell voltage and SoC can be computed as functions of time using Butler-Volmer kinetics approach that has been widely used in past papers.

The state of charge of the electrode at any time can be written using the average concentration of the electrodes as follows:

$$SoC_j(t) = \frac{\bar{x}_{j,ave}(t) - x_{j,ave0\%,}}{x_{j,ave100\%} - x_{j,ave0\%,}} \quad [10]$$

Where $\bar{x}_{j,ave}(t)$ is the volume-averaged scaled concentration in electrode j at time t, which can be obtained through integration as follows:

$$\bar{x}_{j,ave}(t) = \frac{3\int_{r=0}^{R_j} r^2 c_j(r,\,t)dr}{R_j^3 c_{j,\,\max}} \quad [11]$$

By applying a total mass balance of Lithium in the full cell, the SoCs of the individual electrodes can easily be related to the overall capacity and correspondingly SoC of the cell. However, we only explore the variation of SoC of the negative electrode in this work to demonstrate the capability of this approach.

In order to calculate the electrode potential, the Butler–Volmer kinetics equation is used[38]:

$$J_j(t) = c_{j,\,\max}k_j c_e^{0.5}x_{j,s}^{0.5}(1-x_{j,s})^{0.5}\left[\exp\left(\frac{0.5F}{R_uT}\eta_j\right) - \exp\left(-\frac{0.5F}{R_uT}\eta_j\right)\right] \quad [12]$$

Where $x_{j,s} = \frac{c_{j,s}}{c_{j,\,\max}}$ is the stoichiometry or scaled concentration at the surface of electrode j, k is the reaction rate constant, c_e is the electrolyte concentration, R_u is the universal gas constant, T is the

surface temperature and η_j is the overpotential that can be written as:

$$\eta_j = \varphi_{1,j} - \varphi_{2,j} - U_j \quad [13]$$

Here, U is the open circuit potential, which, in general, depends on the electrode material in the cell, and is obtained from the expressions presented in previous papers.[38] The solid phase and liquid phase potentials can be written as:

$$\varphi_{1,p} - \varphi_{1,n} = V_{cell} \quad [14]$$

$$\varphi_{2,p} - \varphi_{2,n} = IR_{cell} \quad [15]$$

Note that the potential difference in the solution phase is modeled as a resistor in this model. Equations 13–15 can be combined and substituted in Eq. 12. Finally, Eq. 12 can be inverted[38] to result in the following equation for the voltage of the cell as a function of time:

$$V_{cell}(t) = U_p - U_n + \frac{2R_uT}{F}\ln\left[\frac{\sqrt{m_p^2+4}+m_p}{2}\right] + \frac{2R_uT}{F}\ln\left[\frac{\sqrt{m_n^2+4}+m_n}{2}\right] + IR_{cell} \quad [16]$$

Where

$$m_p = \frac{I(t)}{Fk_pS_pc_{p,\max}c_e^{0.5}(1-x_{p,s})^{0.5}x_{p,s}^{0.5}} \quad [17]$$

$$m_n = \frac{I(t)}{Fk_nS_nc_{n,\max}c_e^{0.5}(1-x_{n,s})^{0.5}x_{n,s}^{0.5}} \quad [18]$$

and $S_j = 3\varepsilon_jV_j/R_j$ is the total electroactive area of the electrodes.

Equation 16 provides an analytical expression for the cell voltage as a function of time during a charge/discharge process with time-varying current. Note that the concentration field in Eq. 16 comes from Eq. 9, which represents the Green's function solution for the concentration field under time-dependent flux. These equations make it possible to predict the cell voltage as a function of time for any arbitrary charge/discharge current profile, which could comprise both smooth and discontinuous variations of current with time. In addition, the time-dependence of current could be provided to the model either in the form of analytical equations, or discrete experimental data.

Results and Discussion

Model validation.—The analytical model for predicting SoC and voltage curves for time-varying current presented in the mathematical section is validated by comparison against predictions based on numerical simulations as well as experimental data reported in the past. These results are discussed in sub-sections below.

Validation against SPM numerical simulation.—Voltage profile predicted by the analytical model is compared against numerical models for a special case of constant current as well as other time-dependent current profiles. For constant current, a previously reported SPM-based numerical computation tool for constant current charge/discharge (S. Kolluri & V. Subramanian, personal communication, May 17, 2020) is used for comparison. For time-dependent current, a finite-difference based code originally written for solving heat transfer problems is modified and used. In both cases, the governing equation and boundary conditions for solid phase diffusion in a spherical electrode particle (Eqs. 1–4) are discretized in time and space. The concentration at the surface of the electrodes is determined and used to calculate the cell voltage using Eq. 16.

For validation in constant current conditions, a $LiCoO_2$ cell is considered with nominal capacity of 1.78 A-hr. The cutoff voltage for charge and discharge are set to be 4.2 V and 2.8 V, respectively. Values of cell parameters used for comparison against the numerical simulation are taken from Refs. 28, 45 and summarized in Table I. Comparison is carried out for charge and discharge at four different C-rates, as shown in Figs. 2a and 2b, respectively. There is excellent agreement between the analytical model and numerical simulation at each C-rate for both charge and discharge. In each case, the curves for analytical model and numerical simulation are nearly indistinguishable from each other.

Validation of the analytical model is then carried out for time-dependent currents. Two specific current profiles are used—the first one has two cycles of a discharge-rest-charge process, and the second one is a part of the US06 drive cycle commonly used for automotive benchmarking.[46,47] The US06 drive cycle features significant fluctuations in currents representative of realistic driving behavior. Figures 3a and 3b present comparison of the analytical model against numerical simulation for these two current profiles, respectively. In each case, the variation in current with time is also plotted for comparison. Plots show that the analytical model and the numerical simulation are in very good agreement even for complicated time-dependent current profiles.

Validation against other models.—This subsection presents a comparison of the model developed in this paper with other past approaches for calculating the voltage curve. Two past models developed by Smith, et al.[33] and Cen & Kubiak[48] are considered here. Smith, et al.[33] presented a linear Kalman filter approach based on a reduced-order electrochemical model for voltage and SoC estimation. Cen & Kubiak,[48] on the other hand, presented an adaptive observer based on a simplified single particle model (SPM) to predict the voltage and SoC of a Li-ion cell. The

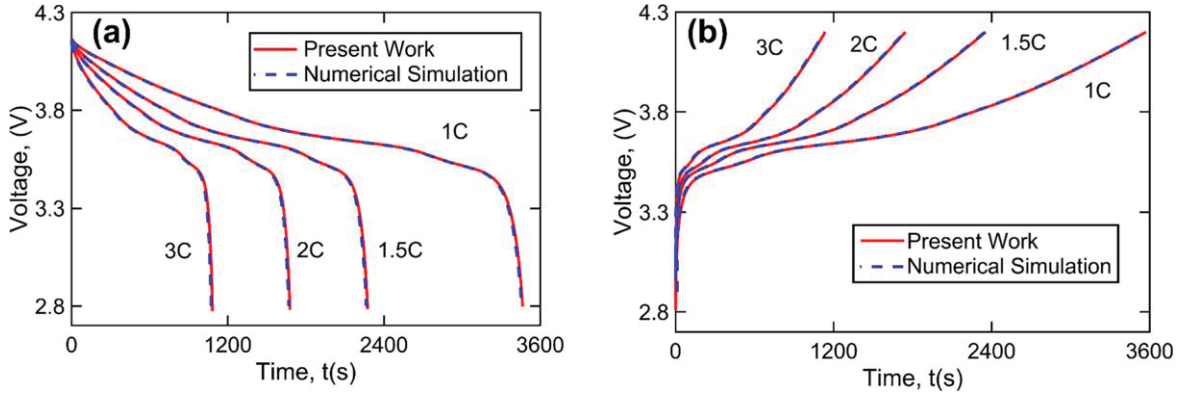

Figure 2. Validation of the analytical model against SPM-based numerical simulations for constant current processes: Voltage as a function of time for (a) discharge, and (b) charge for multiple C-rates.

Table I. Electrochemical and physical properties used in this study.

Properties	Anode	Cathode	Units
R	5×10^{-6}	5×10^{-6}	m
l	4.000×10^{-5}	3.655×10^{-5}	m
D	1.4×10^{-14}	2.0×10^{-14}	$m^2\ s^{-1}$
c_{max}	31080	51830	mol m^{-3}
k	$0.6346667351 \times 10^{-9}$	$0.6306608809 \times 10^{-9}$	$m^{2.5}\ mol^{-0.5}\ s^{-1}$
S	1.6206	1.2974	m^2
$x_{0\%}$	0.005139	0.947659	—
$x_{100\%}$	0.790813	0.359749	—
T	298		K
F	96487		C mol^{-1}
R_u	8.314		J $mol^{-1}\ K^{-1}$
c_e	1200		mol m^{-3}
R_{cell}	0.001		Ω
U_p	$-10.72 \times x^4_{p,s} + 23.88 \times x^3_{p,s} - 16.77 \times x^2_{p,s} + 2.595 \times x_{p,s} + 4.563$		V
U_n	$0.1493 + 0.8493 \times \exp(-61.79 \times x_{n,s}) + .3824 \times \exp(-665.8 \times x_{n,s})$-$\exp(39.42 \times x_{n,s} - 41.92) - 0.03131 \times \operatorname{atan}(25.59 \times x_{n,s} - 4.099) - 0.009434 \times \operatorname{atan}(32.49 \times x_{n,s} - 15.74)$		V

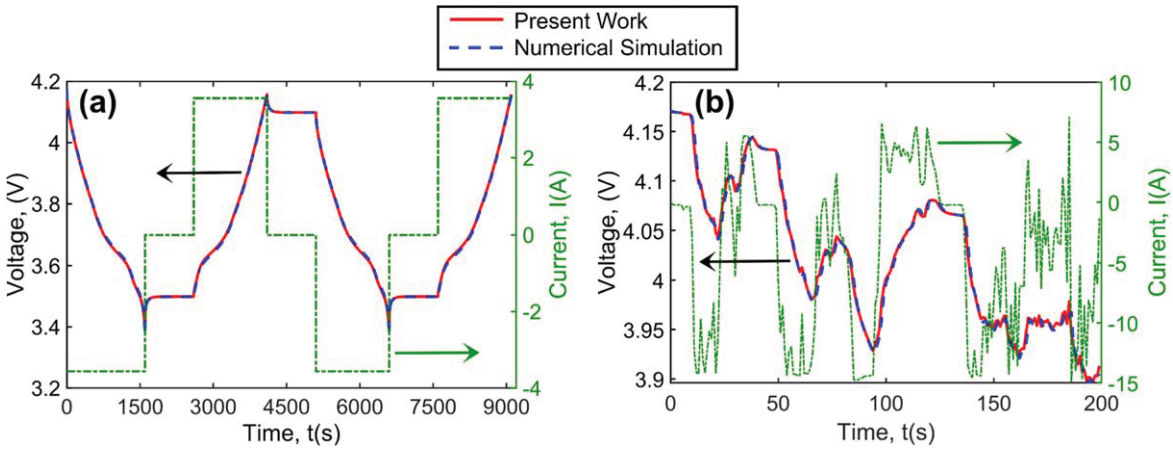

Figure 3. Validation of the analytical model against SPM-based numerical simulations for time-dependent current processes: Voltage as a function of time for (a) discharge-rest-discharge, and (b) dynamic current profile.

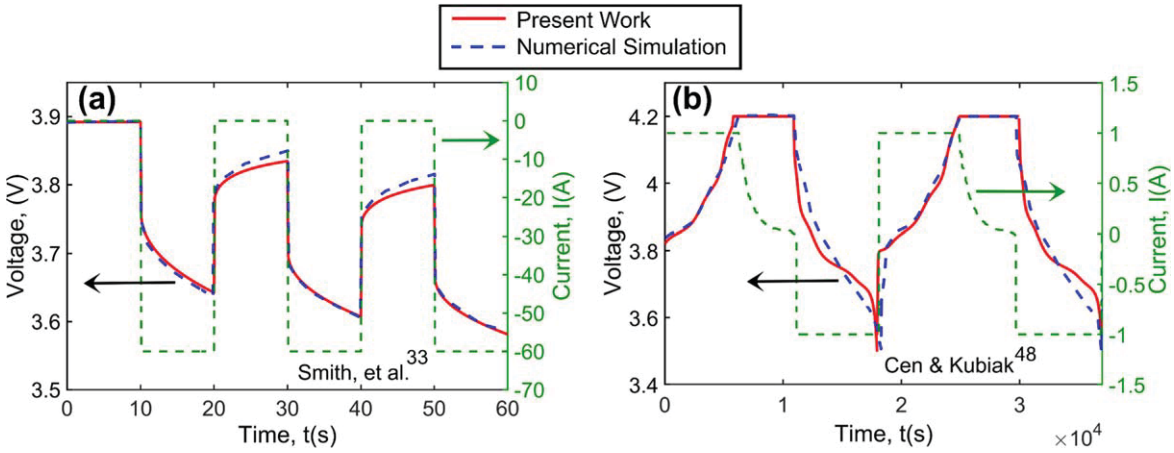

Figure 4. Validation of the analytical model against past numerical models for variable current processes: Voltage as a function of time for (a) discharge-charge process,[33] and (b) discharge-rest-charge process.[48]

electrochemical parameters used for these comparison plots can be found in the corresponding papers.[33,48] Figure 4a plots voltage as a function of time obtained from the analytical model presented here and the past study by Smith, et al.[33] The current profile used for this comparison is also shown on the right axis. Results show good agreement between the two models, with a worst-case disagreement of only around 0.4%. Note that the model presented by Smith, et al.[33] accounts for electrochemical dynamics of the electrolyte, while the present model considers the electrolyte dynamic as a fixed film resistance, which may explain the difference in the voltage peaks between the two models. Similarly, Fig. 4b plots voltage as a function of time for the present analytical model and the past study by Cen & Kubiak[48] for a constant current-constant voltage (CC-CV) process, also shown in the figure. There is a reasonable agreement between the two models. The slight disagreement between the two models is likely due to lack of clarity about the values of initial SoC and stoichiometry for this specific plot used by Cen & Kubiak.[48]

Validation against past experimental data.—Finally, validation of the analytical model is also carried out by comparison with previously reported experimental measurements by Guo, et al.[38] and Smith & Wang.[34] Guo, et al.[38] presented experimental measurement of voltage under a constant discharge rate of C/33 for a pouch cell with a nominal capacity of 1.656 A-hr. Smith and Wang,[34] on the other hand, presented experimental data for a HPPC drive cycle profile for multiple values of initial state of charge. Both papers listed electrochemical properties of the cell used in experiments.[34,38] Using these cell parameters, the analytical model is used to compute the voltage curve for both experiments. Figure 5a presents a comparison between measurements and analytical model for constant current discharge measurements by Guo, et al.[38] There is excellent agreement between the two throughout the entire measurement period. Figure 5b shows a similar comparison for a more complicated current profile used for voltage measurements by Smith and Wang[34] for two different values of the initial SoC. Figure 5b shows that the analytical model is able to successfully predict the voltage profile for the pulsed current profile.

Taken together, the comparison against numerical computation, other past models as well as experimental measurements in a variety of constant and time-varying current conditions provides very good validation of the analytical model presented in the mathematical section.

Applications of the model.—In this section, the Green's function based analytical model is used to predict the voltage and SoC profiles of a cell in a number of operating conditions. Step-function and sinusoidal changes in current over time are considered. In addition, current profiles for two drive cycles—ECE-15 and US06—that represent realistic driving conditions are analyzed. Cell parameters used in all the figures in this section are same as those used in Figs. 2 and 3, and are summarized in Table I.

Step-function current profile.—Cell performance is analyzed under two different step-function current profiles—successive discharge at multiple C-rates (0.5C, 1.5C and 3C) and discharge-charge-discharge

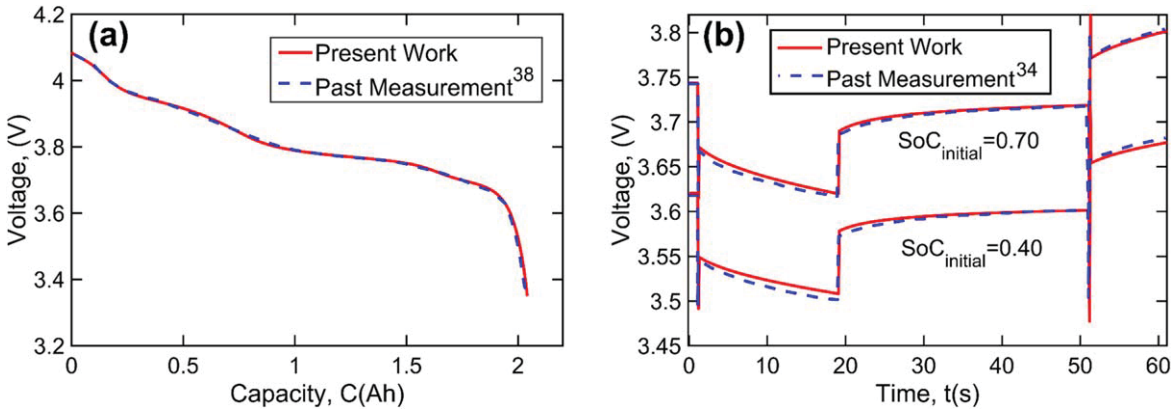

Figure 5. Validation of the analytical model against past experimental measurements: Voltage as a function of time for (a) constant current discharge,[38] and (b) HPPC drive cycle.[34]

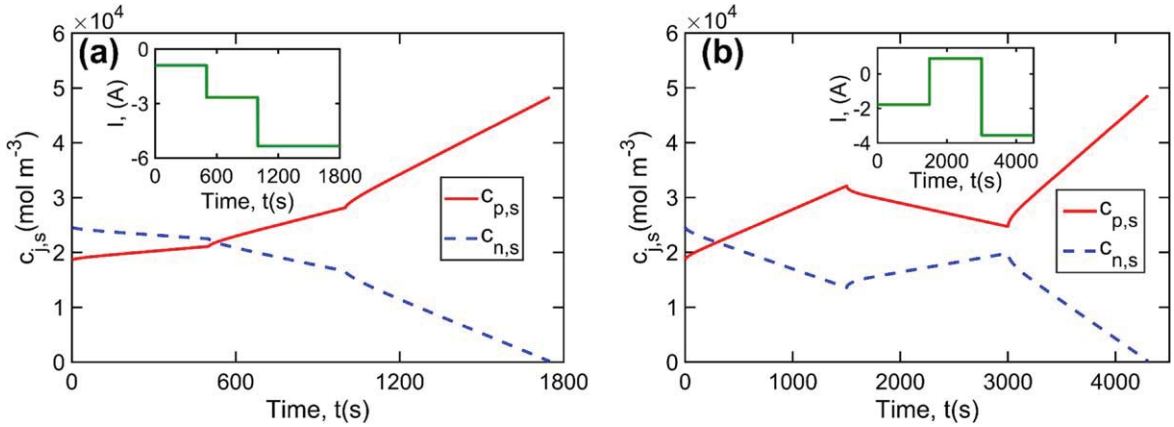

Figure 6. Application of the analytical model for a step-function current profile: Concentration as a function of time for (a) discharge at multiple C-rates, (b) discharge-charge-discharge process.

process. To illustrate the electrochemical phenomena that occurs inside the cell operating under step-function current profiles, surface concentrations on the positive and negative electrodes are computed using Eq. 9 and plotted as a function of time for the two current profiles in Figs. 6a and 6b, respectively. In both cases, the current profile is shown as an inset. As expected, during discharge, concentration on the surface of the negative electrode decreases while concentration on the surface of the positive electrode increases. Further, the rate of change of the concentration goes up as the discharge rate increases. Figure 6b presents a similar plot for a discharge-charge-discharge current profile, also shown as an inset. It is seen that concentration in the positive electrode increases for $t < 1500$ s while the cell discharges, then decreases for $1500\text{ s} < t < 3000$ s while the cell charges, and finally increases again for $t > 3000$ s while the cell discharges. Concentration on the surface of the negative electrode shows similar behavior that is consistent with the current profile. As expected, the slopes of the curves are larger for the second discharge than the first one due to the greater rate of the second discharge.

Based on the concentration fields computed by the Green's function approach, as illustrated in Fig. 6, the voltage and SoC as functions of time are computed using Eqs. 16 and 10, respectively. Figures 7a and 7b present voltage and average SoC at the negative electrode for the two current profiles discussed in Fig. 6. It is seen from Fig. 7a that the voltage decreases continuously due to the discharge process, and shows a change in the rate of reduction when the discharge rate changes from 0.5C to 1.5C, and then to 3C at 500 s and 1000 s, respectively. This is consistent with both the current profile as well as the concentration profile shown in Fig. 6a. The volume-averaged SoC of the negative electrode given by Eq. 10, also shown in Fig. 6a, is consistent with the current and voltage profiles. The SoC decreases throughout, as expected, and at the greatest rate for the highest C-rate, also as expected.

A similar plot for the discharge-charge-discharge profile is shown in Fig. 7b. In this case, as expected, both voltage and SoC decrease in the discharge period, increase in the charge period and finally decrease in the last period of discharge at a greater rate due to the greater C-rate.

These plots demonstrate the capability of the Green's function based analytical model to predict the voltage and SoC variation in the cell over time due to current profiles comprising of step functions.

Sinusoidal current profile.—The analytical model is used next to investigate the voltage/SoC behavior of a Li-ion cell operating under two sinusoidal current profiles, which may be the case for Electrochemical Impedance Spectroscopy (EIS), or for alternating current (AC) charging/discharging of the cell. Two different sinusoidal current profiles are considered. Figure 8 presents plots for voltage and SoC of a Li-ion cell under a sinusoidal discharge current profile of $I(t) = I_0(1 + \sin \omega t)$, where $I_0 = -1.76$ A corresponds to 1C discharge. This current profile is a combination of AC and DC that discharges the cell throughout the time period. This specific current profile is chosen in this study to demonstrate the applicability of this approach for complicated dynamic current profiles. Such profiles have been recently used for battery diagnostics.[49] Figures 8a and 8b plot cell voltage and SoC, respectively, as functions of time for three different values of frequency, ω. The current profiles are also shown as an inset. While both voltage and SoC decrease over time, as expected,

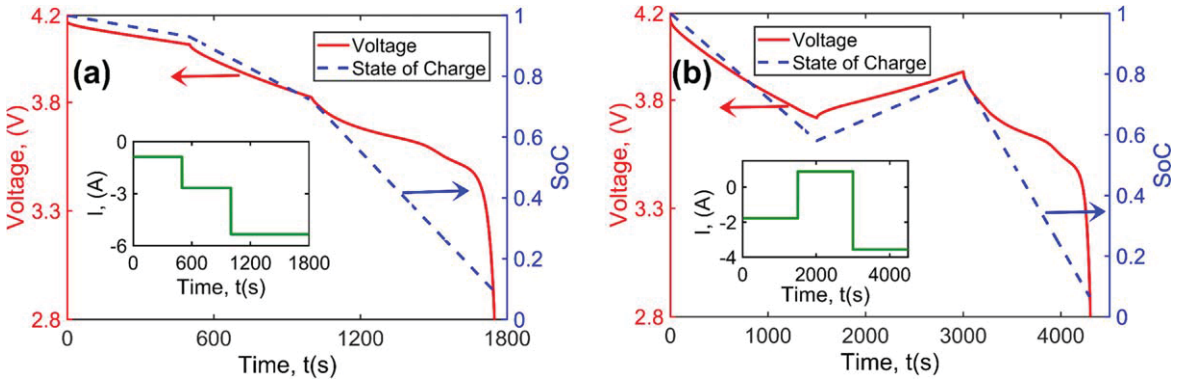

Figure 7. Application of the analytical model for a step-function current profile: Voltage and SOC as functions of time for (a) discharge at multiple C-rates, (b) discharge-charge-discharge process.

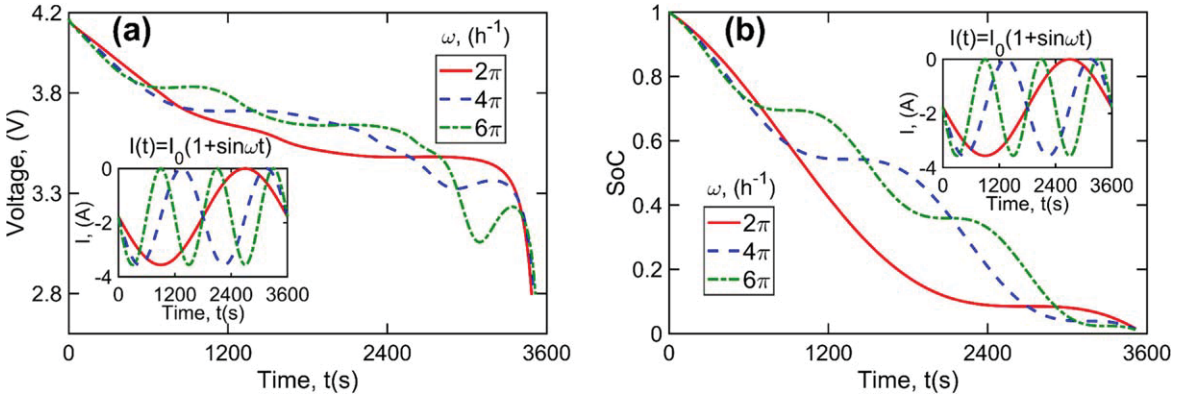

Figure 8. Application of the analytical model for a combination of AC-DC profile, $I(t) = I_0\ (1 + \sin\ \omega t)$: (a) Voltage and (b) SOC as functions of time.

periodicity in the voltage and SoC is also seen, with the number of crests and troughs being consistent with the current profile for each frequency. At each crest, when the discharge current becomes zero for an instant, the voltage curve becomes flat momentarily. It is interesting that for each frequency considered here, the cell fully discharges at about the same time, which is because the integral of the current profile over the time period remains the same for all three frequencies considered here and the DC component of the current primarily causes the reduction in voltage and SoC. Figure 8b presents a plot of average SoC at the negative electrode as a function of time for different values of frequency. The sinusoidal footprint of the current profile is also easily seen in the SoC curve, where, similar to voltage, the SoC curve flattens momentarily when the current becomes zero.

A second type of sinusoidal current profile $I(t) = I_0 \sin \omega t$ is also considered. This profile is representative of AC charge/discharge, which is commonly used in EIS measurements for investigating the electrochemical processes that occur inside the cell. Based on this current profile, the cell is periodically subjected to both charge and discharge. Figures 9a and 9b plot voltage and SoC, respectively, as functions of time for this current profile with multiple values of frequency. The current profile is also shown as an inset. Unlike the previous case where the voltage and SoC gradually reduce over time due to the discharge-only nature of the process, in this case, both voltage and SoC oscillate harmonically due to the charge-discharge nature of the current profile. As the current frequency increases, the number of times that voltage and SoC plots oscillate also increases. EIS typically uses a very low current amplitude to probe only the linear response of the physical processes inside the cell, whereas a large amplitude of current used here causes a corresponding large amplitude of voltage and SoC.

ECE-15 and US06 current profiles.—The current profiles considered so far are ideal ones, whereas current profiles may be a lot more complicated in realistic charge/discharge conditions, for example in automotive applications. The Green's function based analytical model presented in the mathematical section is next used to predict the behavior of a Li-ion cell operating under two dynamic load cycles—ECE-15 and US06. Both are representative of conditions that may be encountered in a realistic electric vehicle battery pack and are commonly used as benchmarks for studying battery performance. Figures 10a and 10b present voltage and SoC plots for an ECE-15[50] current profile, which is also plotted in both Figures for comparison. Both voltage and SoC plots closely follow the changes in the current profile. In general, the voltage and SoC curves are smoother than the current profile due to the diffusion time constants—it takes a finite time for voltage and SoC curves to respond to fluctuations in current. In some instances, such as around $t = 140$ s, the voltage and SoC continue to drop even after the magnitude of the discharge current has passed its peak, which is likely because the cell is still being discharged even though the magnitude of the discharge current is reducing with time. Higher discharge current causes a larger voltage drop due to cell polarization. Voltage drop due to cell polarization continues to decrease as the magnitude of the current decreases, leading to an increase in the voltage of the cell after 145 s. It is interesting to see that whenever the current becomes zero, the voltage still changes for a little while, but SoC becomes flat almost instantaneously, which is expected as the cell reverts back to its open circuit potential.

The second drive cycle is even more complicated, and illustrates the capability of the Green's function based analytical model to predict voltage and SoC for very complicated and dynamic drive profiles. The US06 drive cycle is commonly used to represent current profile for an electric vehicle battery pack for realistic driving conditions.[46,47] The drive profiles are scaled for an 1.78Ah cell, used in the analytical model. Figures 11a and 11b plot voltage and SoC, respectively, as functions of time for the US06 current

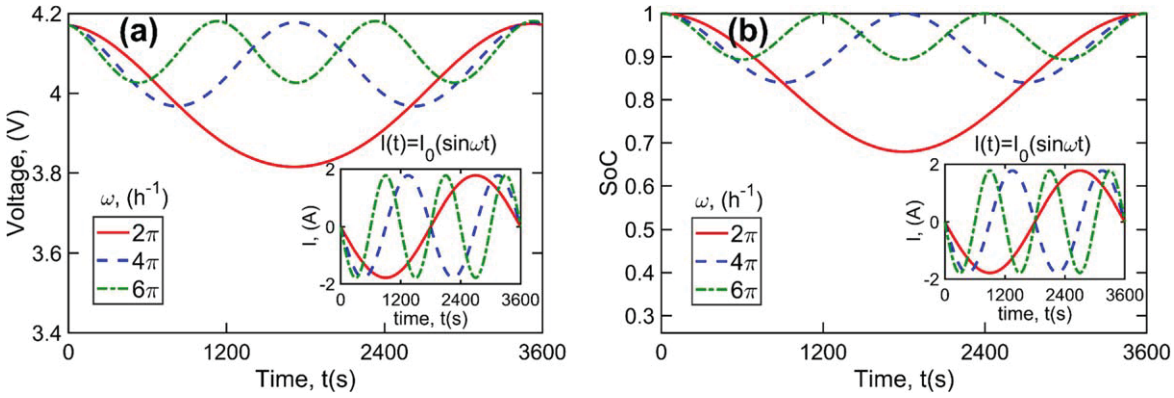

Figure 9. Application of the model for a harmonic current profile $I(t) = I_0(\sin \omega t)$: (a) Voltage and (b) SOC as functions of time.

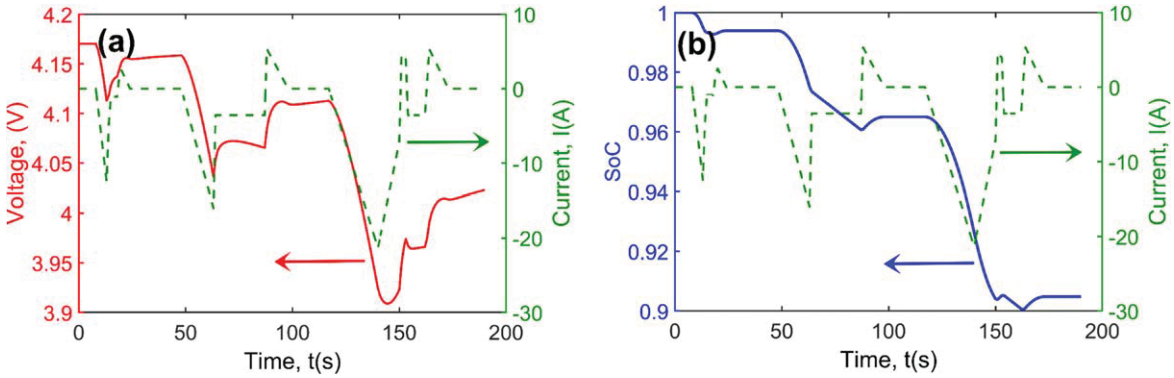

Figure 10. Cell response predicted by the analytical model for a realistic process based on ECE-15 drive cycle[49]: (a) Voltage and (b) SoC as functions of time.

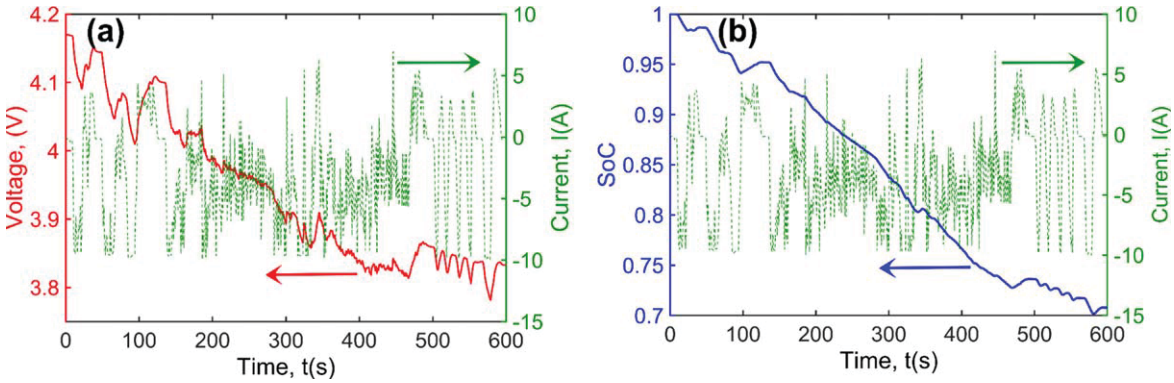

Figure 11. Cell response predicted by the analytical model for a realistic process based on US06 drive cycle: (a) Voltage and (b) SoC as functions of time.

profiles, also shown in these Figures. While the current profile is very dynamic and includes multiple, sharp changes, including between charge and discharge, Figs. 11a and 11b demonstrate the capability of the analytical model to follow the current profile and predict the cell voltage and SoC as functions of time. The cell voltage and SoC are seen to follow the fluctuations in current, and generally decrease over time because the applied current is negative (discharge) for most of the duration. Note that the concentration profile and consequently the voltage and SoC are determined analytically even for these very complicated profiles, which results in fast computation without the need for mesh generation.

Conclusions

The voltage and SoC computation presented here is carried out using a Green's function based exact analytical solution for the concentration profile in the electrodes for an arbitrary time-dependent current profile. This analytical approach agrees well with numerical simulations for a variety of conditions and may be easier to implement in practical battery management systems, especially with controllers containing limited memory. The individual electrode SoC can easily be related to the overall capacity/SoC of the cell. Even for very complicated current profiles, the analytical model is shown to be able to accurately predict the voltage and SoC changes in the cell over time. It should be noted that the model presented here is based on a single spherical particle model, and therefore is valid within the range of validity of the SPM model, i.e. low to moderate C-rates. Also note that the Green's function approach is inherently valid only for linear systems. Non-linearities such as concentration-dependent diffusivities, which may be significant for modeling of certain battery chemistries, sizes and form factors are not accounted for by the model. Finally, the model is

isothermal, and does not account for the impact of temperature on diffusion or kinetic processes. Note that the analytical solution presented here can be used as a basis for state estimation algorithms such as Kalman filter approach for SoC estimation. Furthermore, the solution can also be coupled with the energy balance equation to account for thermal effects. This work is expected to contribute towards the improvement of battery management systems (BMS) for a variety of applications.

Acknowledgments

This material is based upon work supported by CAREER Award No. CBET-1554183 from the National Science Foundation. Authors would like to gratefully acknowledge Dr Suryanarayana Kolluri and Prof. Venkat Subramanian for sharing their constant current SPM code for validation of the present model.

ORCID

Ankur Jain https://orcid.org/0000-0001-5573-0674

References

1. H. Rahimi-Eichi, U. Ojha, F. Baronti, and M. Y. Chow, "Battery management system: an overview of its application in the smart grid and electric vehicles." *IEEE Ind. Electron. Mag.*, **7**, 4 (2013).
2. T. R. Tanim, C. D. Rahn, and C. Y. Wang, "State of charge estimation of a lithium ion cell based on a temperature dependent and electrolyte enhanced single particle model." *Energy*, **80**, 731 (2015).
3. Y. Xing, E. W. Ma, K. L. Tsui, and M. Pecht, "Battery management systems in electric and hybrid vehicles." *Energies*, **4**, 1840 (2011).
4. L. Lu, X. Han, J. Li, J. Hua, and M. Ouyang, "A review on the key issues for lithium-ion battery management in electric vehicles." *J. Power Sources*, **226**, 272 (2013).
5. R. Xiong, J. Cao, Q. Yu, H. He, and F. Sun, "Critical review on the battery state of charge estimation methods for electric vehicles." *IEEE Access*, **6**, 1832 (2017).
6. M. Corno, N. Bhatt, S. M. Savaresi, and M. Verhaegen, "Electrochemical model-based state of charge estimation for Li-ion cells." *IEEE Trans. Control Syst. Technol.*, **23**, 117 (2014).
7. Y. Xiao, C. Lin, and B. Fahimi, "Online state of charge estimation in electro-chemical batteries: application of pattern recognition techniques." *2013 Twenty-Eighth Annual IEEE Applied Power Electronics Conference and Exposition (APEC)* (IEEE) p. 2474 (2013).
8. C. Lin, A. Tang, and J. Xing, "Evaluation of electrochemical models based battery state-of-charge estimation approaches for electric vehicles." *Appl. Energy*, **207**, 394 (2017).
9. F. Yang, Y. Xing, D. Wang, and K. L. Tsui, "A comparative study of three model-based algorithms for estimating state-of-charge of lithium-ion batteries under a new combined dynamic loading profile." *Appl. Energy*, **164**, 387 (2016).
10. Y. Xing, W. He, M. Pecht, and K. L. Tsui, "State of charge estimation of lithium-ion batteries using the open-circuit voltage at various ambient temperatures." *Appl. Energy*, **113**, 106 (2014).
11. H. He, R. Xiong, and H. Guo, "Online estimation of model parameters and state-of-charge of $LiFePO_4$ batteries in electric vehicles." *Appl. Energy*, **89**, 413 (2012).
12. K. S. Ng, C. S. Moo, Y. P. Chen, and Y. C. Hsieh, "Enhanced coulomb counting method for estimating state-of-charge and state-of-health of lithium-ion batteries." *Appl. Energy*, **86**, 1506 (2009).
13. X. Hu, S. Li, H. Peng, and F. Sun, "Robustness analysis of State-of-Charge estimation methods for two types of Li-ion batteries." *J. Power Sources*, **217**, 209 (2012).
14. J. Zhang and J. Lee, "A review on prognostics and health monitoring of Li-ion battery." *J. Power Sources*, **196**, 6007 (2011).
15. A. J. Salkind, C. Fennie, P. Singh, T. Atwater, and D. E. Reisner, "Determination of state-of-charge and state-of-health of batteries by fuzzy logic methodology." *J. Power Sources*, **80**, 293 (1999).
16. J. D. Kozlowski, "Electrochemical cell prognostics using online impedance measurements and model-based data fusion techniques." *2003 IEEE Aerospace Conference Proceedings (Cat. No. 03TH8652)* (IEEE), **7**, 3257 (2003).
17. L. Kang, X. Zhao, and J. Ma, "A new neural network model for the state-of-charge estimation in the battery degradation process." *Appl. Energy*, **121**, 20 (2014).
18. J. C. A. Anton, P. J. G. Nieto, C. B. Viejo, and J. A. V. Vilán, "Support vector machines used to estimate the battery state of charge." *IEEE Trans. Power Electron.*, **28**, 5919 (2013).
19. B. Y. Liaw, G. Nagasubramanian, R. G. Jungst, and D. H. Doughty, "Modeling of lithium ion cells—a simple equivalent-circuit model approach." *Solid State Ionics*, **175**, 835 (2004).
20. R. Xiong, F. Sun, Z. Chen, and H. He, "A data-driven multi-scale extended Kalman filtering based parameter and state estimation approach of lithium-ion polymer battery in electric vehicles." *Appl. Energy*, **113**, 463 (2014).
21. G. L. Plett, "Extended Kalman filtering for battery management systems of LiPB-based HEV battery packs: Part I. Background." *J. Power Sources*, **134**, 252 (2004).
22. G. L. Plett, "Extended Kalman filtering for battery management systems of LiPB-based HEV battery packs: Part II. Modeling and identification." *J. Power Sources*, **134**, 262 (2004).
23. G. L. Plett, "Extended Kalman filtering for battery management systems of LiPB-based HEV battery packs: Part III. State and parameter estimation." *J. Power Sources*, **134**, 277 (2004).
24. J. Lee, O. Nam, and B. H. Cho, "Li-ion battery SOC estimation method based on the reduced order extended Kalman filtering." *J. Power Sources*, **174**, 9 (2007).
25. M. Verbrugge and E. Tate, "Adaptive state of charge algorithm for nickel metal hydride batteries including hysteresis phenomena." *J. Power Sources*, **126**, 236 (2004).
26. I. S. Kim, "The novel state of charge estimation method for lithium battery using sliding mode observer." *J. Power Sources*, **163**, 584 (2006).
27. X. Hu, F. Sun, and Y. Zou, "Estimation of state of charge of a lithium-ion battery pack for electric vehicles using an adaptive Luenberger observer." *Energies*, **3**, 1586 (2010).
28. M. Doyle, T. F. Fuller, and J. Newman, "Modeling of galvanostatic charge and discharge of the lithium/polymer/insertion cell." *J. Electrochem. Soc.*, **140**, 1526 (1993).
29. M. Rashid and A. Gupta, "Mathematical model for combined effect of SEI formation and gas evolution in Li-ion batteries." *ECS Electrochem. Lett.*, **3**, A95 (2014).
30. M. Rashid and A. Gupta, "Effect of relaxation periods over cycling performance of a Li-ion battery." *J. Electrochem. Soc.*, **162**, A3145 (2015).
31. W. Du, A. Gupta, X. Zhang, A. M. Sastry, and W. Shyy, "Effect of cycling rate, particle size and transport properties on lithium-ion cathode performance." *Int. J. Heat Mass Transfer*, **53**, 3552 (2010).
32. K. A. Smith, C. D. Rahn, and C. Y. Wang, "Control oriented 1D electrochemical model of lithium ion battery." *Energy Convers. Manage.*, **48**, 2565 (2007).
33. K. A. Smith, C. D. Rahn, and C. Y. Wang, "Model-based electrochemical estimation and constraint management for pulse operation of lithium ion batteries." *IEEE Trans. Control Syst. Technol.*, **18**, 654 (2009).
34. K. Smith and C. Y. Wang, "Solid-state diffusion limitations on pulse operation of a lithium ion cell for hybrid electric vehicles." *J. Power Sources*, **161**, 628 (2006).
35. A. Subramaniam, S. Kolluri, C. D. Parke, M. Pathak, S. Santhanagopalan, and V. R. Subramanian, "Properly Lumped Lithium-ion battery models: a Tanks-in-Series approach." *J. Electrochem. Soc.*, **167**, 013534 (2020).
36. A. Jokar, B. Rajabloo, M. Désilets, and M. Lacroix, "Review of simplified Pseudo-two-Dimensional models of lithium-ion batteries." *J. Power Sources*, **327**, 44 (2016).
37. M. Doyle and J. Newman, "Analysis of capacity–rate data for lithium batteries using simplified models of the discharge process." *J. Appl. Electrochem.*, **27**, 846 (1997).
38. M. Guo, G. Sikha, and R. E. White, "Single-particle model for a lithium-ion cell: thermal behavior." *J. Electrochem. Soc.*, **158**, A122 (2011).
39. X. Han, M. Ouyang, L. Lu, and J. Li, "Simplification of physics-based electro-chemical model for lithium ion battery on electric vehicle. Part I: diffusion simplification and single particle model." *J. Power Sources*, **278**, 802 (2015).
40. T. R. Tanim, C. D. Rahn, and C. Y. Wang, "A reduced order electrolyte enhanced single particle lithium ion cell model for hybrid vehicle applications." *2014 American Control Conference* (IEEE) p. 141 (2014).
41. W. Luo, C. Lyu, L. Wang, and L. Zhang, "A new extension of physics-based single particle model for higher charge–discharge rates." *J. Power Sources*, **241**, 295 (2013).
42. S. Santhanagopalan and R. E. White, "Online estimation of the state of charge of a lithium ion cell." *J. Power Sources*, **161**, 1346 (2006).
43. M. Parhizi and A. Jain, "Analytical modeling of solid phase diffusion in single-layer and composite electrodes under time-dependent flux boundary condition." *J. Electrochem. Soc.*, **167**, 060528 (2020).
44. M. Guo and R. E. White, "An approximate solution for solid-phase diffusion in a spherical particle in physics-based Li-ion cell models." *J. Power Sources*, **198**, 322 (2012).
45. P. Ramadass, B. Haran, P. M. Gomadam, R. White, and B. N. Popov, "Development of first principles capacity fade model for Li-ion cells." *J. Electrochem. Soc.*, **151**, A196 (2004).
46. P. Keil, M. Englberger, and A. Jossen, "Hybrid energy storage systems for electric vehicles: an experimental analysis of performance improvements at subzero temperatures." *IEEE Trans. Veh. Technol.*, **65**, 998 (2015).
47. G. Zhang, S. Ge, X. G. Yang, Y. Leng, D. Marple, and C. Y. Wang, "Rapid restoration of electric vehicle battery performance while driving at cold temperatures." *J. Power Sources*, **371**, 35 (2017).
48. Z. Cen and P. Kubiak, "Lithium-ion battery SOC/SOH adaptive estimation via simplified single particle model." *Int. J. Energy Res.*, available at (2020).
49. L. Teo, M. Pathak, S. Kolluri, N. Dawson-Elli, D. T. Schwartz, and V. R. Subramanian, An analysis of transient impedance-like diagnostic signals in batteries, ECS Meeting Abstract Volume MA2018–02 (2018), available at https://iopscience.iop.org/article/10.1149/MA2018-02/25/872, last accessed 07/09/2020.
50. T. Sarıkurt, M. Ceylan, and A. Balikçi, "An analytical battery state of health estimation method." *2014 IEEE 23rd International Symposium on Industrial Electronics (ISIE)* (IEEE) p. 1605 (2014).